Resonance Raman study of the *A*-band short-time photodissociation dynamics of 2-iodothiophene

Hai-Lin Zhu and Jian Liu
Department of Chemistry, Zhejiang Sci-Tech University, Hangzhou, People's Republic of China 310018

Xuming Zheng[a),b)]
Department of Chemistry, Zhejiang Sci-Tech University, Hangzhou, People's Republic of China 310018
and State Key Laboratory of ATMMT (MOE), Zhejiang Sci-Tech University, Hangzhou,
People's Republic of China 310018

David Lee Phillips[a),c)]
Department of Chemistry, The University of Hong Kong, Pokfulam Road, Hong Kong, SAR,
People's Republic of China

Resonance Raman spectra were obtained for 2-iodothiophene in cyclohexane solution with excitation wavelengths in resonance with the *A*-band absorption spectrum. These resonance Raman spectra indicate that the Franck-Condon region photodissociation dynamics have multidimensional character with motion mainly along the nominal symmetric C=C stretch of the thienyl ring and accompanied by a moderate amount of motion along the nominal symmetric CSC stretch, the nominal antisymmetric CSC stretch, and the nominal C–I stretch vibrational modes. A preliminary resonance Raman intensity analysis was done for the *A*-band resonance Raman spectra of 2-iodothiophene. These results were compared to previous results for related iodobenzene and iodoalkane molecules that also contain a C–I chromophore and the similarities and differences in the short-time photodissociation dynamics were discussed. © *2006 American Institute of Physics.*
[DOI: 10.1063/1.2236118]

I. INTRODUCTION

The *A*-band photodissociation of iodoalkanes has long been studied as a model for direct photodissociation reactions. Many experimental and theoretical investigations have been done to examine the photodissociation dynamics, the energy disposal, and the branching ratio of the $^3Q_0$ and $^1Q_1$ curve crossing of the direct photodissociation reactions of iodoalkanes.[1–65] The *A*-band absorption of iodoalkanes arises due to the promotion of a nonbonding electron from the iodine atom to the antibonding σ^* molecular orbital localized on the C–I bond ($n \rightarrow \sigma^*$ transition). Excitation within the *A*-band absorption results in a direct dissociation of the C–I bond that leads to the formation of an alkyl radical and the iodine atoms in their ground I($^2P_{3/2}$) and spin-orbit I*($^2P_{1/2}$) excited states. The $n \rightarrow \sigma^*$ transition in iodoalkanes is composed of three overlapping transitions from the ground state to the repulsive $^3Q_1$, $^3Q_0$, and $^1Q_1$ states. The $^3Q_0$ transition is located near the middle of the absorption band and contains about 70%–80% of the oscillator strength, while the $^3Q_1$ and $^1Q_1$ transitions have the remaining oscillator strength and are located near the red and blue edges of the absorption band of iodomethane, respectively.[1] Real-time femtosecond pump-probe experiments have shown that the iodomethane photodissociation is complete in less than 100 fs.[2,3] The vibrational and rotational state distributions of

the alkyl radical photoproduct and I*/I branch ratio have been measured using several experimental methods.[4–28] These experimental results indicate that as the alkyl group gets larger and/or more branched in structure then the degree of internal excitation of the alkyl radical photofragment and the $^3Q_0$ to $^1Q_1$ curve crossing probability increases. Theoretical models of iodomethane photodissociation with various potential energy surfaces have been used with reasonable success to interpret and simulate much of the experimental data available for the iodomethane *A*-band photodissocation.[29–38] Resonance Raman spectroscopy was used to examine the short-time photodissociation dynamics of iodoalkanes.[39–65] The resonance Raman spectra were dominated by a long overtone progression in the C–I stretch mode and accompanied by small combination band progression(s) of other modes plus C–I stretch overtones. These results show that as the mass increases and/or the structure becomes more branched, then the intensity in the nominal non-C–I stretch combination bands with the C–I stretch overtones increases relative to the C–I stretch overtone progression intensity.

Aryl iodides are another type of interesting molecules that have received attention for their underlying direct or indirect photodissociation reaction mechanisms.[66–79] Photofragment translation spectroscopy studies show that there are two types of dissociative states in the absorption region between 320 and 220 nm for iodobenzene.[66–69] One is the $^3(n, \sigma^*)$ state resulting from the promotion of a nonbonding electron from the iodine atom valence shell to an antibonding

a)Authors to whom correspondence should be addressed.
b)Fax: 86-0571-86843000. Electronic mail: zhengxuming126@126.com
c)Fax: 852-2857-1586. Electronic mail: phillips@hkucc.hku.hk

125, 054510-1

σ^* orbital localized along the C–I bond and this state is similar to those responsible for the A-band photodissociation observed in iodoalkanes. Excitation to this state of iodobenzene leads to a rapid direct dissociation that produces a phenyl radical and an iodine atom. The other dissociative state is the $^3(\pi, \pi^*)$ bound state of the benzene ring and this is overlapped to some extent with the $^3(n, \sigma^*)$ state. Excitation to the $^3(\pi, \pi^*)$ state of a halobenzene leads to an indirect photodissociation that occurs due to a potential energy surface intersection between the $^3(\pi, \pi^*)$ state and the $^3(n, \sigma^*)$ state.[66,67,70,71] A state-selective investigation showed that the iodobenzene molecule in the $^3(n, \sigma^*)$ state dissociates much faster than molecular rotation, whereas the predissociation in the $^3(\pi, \pi^*)$ state occurred on a time scale comparable to molecular rotation.[72–75] Resonance Raman spectroscopy was used to find vibrational mode-specific information on the Franck-Condon photodissociation dynamics of iodobenzene.[78,79]

In this paper we report a preliminary resonance Raman intensity analysis study of 2-iodothiophene in cyclohexane solution. 2-iodothiophene is a prototypical heterocyclic aromatic molecule that has a strong absorption band near 243 nm. The $\pi \rightarrow \pi^*$ transition of the thienyl ring in 2-iodothiophene is similar to that of the benzene ring in iodobenzene. This allows us to examine how the different types of aromatic rings alter the Franck-Condon region photodissociation dynamics of aromatic iodides. We note that mono-or multihalothiophenes are also important organic reagents that are useful in material science and organic synthesis.[80–82] However, their photochemical reactions and mechanisms are not well-understood and the present study represents a modest beginning to better understand the photodissociation reactions of halothiophenes. The photochemical isomerization of thiophene derivatives were also studied recently using *ab initio* methods.[83] The resonance Raman spectra of 2-iodothiophene will allow us to examine the Franck-Condon region photodissociation dynamics following A-band excitation of 2-iodothiophene and these results will be compared analogous resonance Raman studies for the photodissociation dynamics of iodobenzene and iodoalkane molecules that also contain a C–I chromophore. This comparison will examine how the differing aromatic and/or alkyl moieties influence the Franck-Condon region photodissociation dynamics.

II. EXPERIMENTAL AND COMPUTATIONAL METHODS

A. FTIR, FT-Raman, and resonance Raman experiments

The Fourier transition infrared (FTIR) spectrum of 2-iodothiophene in neat liquid was acquired with 2 cm^{-1} resolution by a Nicolet Avatar 370 FTIR spectrometer. The FT-Raman spectrum of neat liquid 2-iodothiophene was obtained with 2 cm^{-1} resolution and 1064 nm excitation using a Thermo Nicolet FT-Raman 960 spectrometer. The resonance Raman experiments used samples with concentrations in the $0.007-0.015$ M range for 2-iodothiophene in cyclohexane solvent. The power dependence of the resonance Raman spectra was tested and a low power was used during the

resonance Raman measurements to avoid unwanted ground state depletion or multiphoton processes. The use of high peak powers can lead to the depletion of the ground state species and cause the Raman band intensities of sample relative to those of solvent to change when the laser power increases too much. Higher peak power can also produce more photochemical intermediates or cause multiphoton processes to occur during the laser pulse. These will also interfere with absolute Raman cross section measurements.[84]

The methods and experimental apparatus used for the resonance Raman experiments have been described elsewhere[54–64] so only a short description will be given here. The harmonics of a nanosecond Nd:YAG (yttrium aluminum garnet) laser and their hydrogen Raman shifted laser lines produced the excitation wavelengths used in the resonance Raman experiments. The excitation laser beam was loosely focused to about a 0.5 mm diameter spot size onto a flowing liquid stream of sample and a backscattering geometry was used for sample excitation and for the collection of the Raman scattered light by reflective optics. The Raman scattered light was imaged through a depolarizer and entrance slit of a 0.5 m spectrograph whose grating dispersed the light onto a liquid nitrogen cooled charge-coupled device (CCD) mounted on the exit of the spectrograph. The CCD acquired the Raman signal for about 90–120 s before being read out to an interfaced personal computer (P.C.). About 10–30 of these readouts were summed to obtain the resonance Raman spectrum. The Raman shifts of the resonance Raman spectra were calibrated using the known vibrational frequencies of the cyclohexane solvent Raman bands and the solvent Raman bands were subtracted from the resonance Raman spectra using an appropriately scaled solvent spectrum. The spectra of an intensity calibrated deuterium lamp were used to correct the resonance Raman spectral intensities for the variation in the detection efficiency as a function of wavelength. Portions of the resonance Raman spectra were fitted to a base line plus a sum of Lorentzian bands to obtain the integrated areas of the Raman bands.

The absolute Raman cross sections of the 2-iodothiophene resonance Raman spectra were determined relative to the 802 cm^{-1} Raman band of the cyclohexane solvent. An ultraviolet/visible (UV/vis) spectrometer was used to determine the concentrations of the 2-iodothiophene sample before and after each measurement and the absorption spectra changed by $<5\%$ due to photodecomposition and/or solvent evaporation. The absolute Raman cross sections were computed using the average concentration before and after three measurements and finding the mean of three trials to get a final value for the excitation wavelengths determined.

B. Time-dependent wave packet calculations to model the resonance Raman intensities and absorption spectrum

The absorption spectrum and resonance Raman intensities were simulated using Heller's time-dependent wave packet approach to resonance Raman scattering[85–87] and the absorption spectrum was calculated using the following expression:

$$\sigma_A(E_L) = (4\pi e E_L M_0^2/3n\hbar c)\int_{-\infty}^{\infty} G(\delta)d\delta\,\mathrm{Re}\int_0^{\infty} dt\langle 0|0(t)\rangle$$

$$\times[\exp[i(E_L+\varepsilon_0)]t/\hbar]\exp[-\Gamma t/\hbar],$$

and the resonance Raman intensities were calculated using the following formula:

$$\sigma_A(E_L) = (8\pi e^4 E_S^3 E_L M_0^4/9\hbar^6 c^4)\int_{-\infty}^{\infty} G(\delta)d\delta$$

$$\times\left|\int_0^{\infty} dt\langle f|0(t)\rangle[\exp[i(E_L+\varepsilon_0)]t/\hbar]\right.$$

$$\left.\times\exp[-\Gamma t/\hbar]\right|^2,$$

where E_L is the incident photon energy, M_0 is the transition length evaluated at the equilibrium geometry, f is the final state for the Raman scattering, and n is the solvent index of refraction. The term $\exp[-\Gamma t/\hbar]$ is a homogeneous damping function that has contributions from the excited state population decay and pure dephasing. $G(\delta)$ is an inhomogeneous distribution of transition energies. $|0(t)\rangle = e^{-iHt/\hbar}|0\rangle$ which is $|0\rangle$ propagated on the excited state surface for a time t and H is the excited state vibrational Hamiltonian.

The ground and excited state potential energy surfaces were simulated by employing harmonic oscillators with their minima set apart by an amount Δ (with dimensionless units for the ground state normal coordinates). This simple model did not employ Duschinsky rotation[86,87] of the normal modes and the ground and excited state harmonic oscillators had the same vibrational frequency. The resonance Raman intensities of the first several overtones as well as the combination bands and the absorption spectrum are determined mainly by the slope of the excited state surface in the Franck-Condon region in the absence of any vibrational recurrences. The featureless gas and solution phase A-band absorption spectra of 2-iodothiophene suggest that the total electronic dephasing and/or population decay takes place prior to the first vibrational recurrence of any Franck-Condon active modes. For the resonance Raman bands observed in our experimental spectra, the $\langle f|I(t)\rangle$ overlaps decay and have a negligible value after 30 fs. The effects of solvent dephasing were crudely accounted for by using a simple exponential decay term ($\exp[-t/\tau]$). The bound harmonic oscillator model employed here only provides a convenient way to simulate the Franck-Condon region portion of the excited state surface that determines the resonance Raman intensities and absorption spectrum and does not in any way imply that the excited state is actually bound.

C. Density functional theory calculations

Density functional theory (DFT) calculations[88,89] were done to find the optimized geometry and vibrational frequencies as well as the electronic transition energies for the ground or excited electronic states of 2-iodothiophene. Complete geometry optimization and vibrational frequency computations were calculated by using the B3LYP/Sadlej cc-PVTZ level of theory with a C_s symmetry, while the
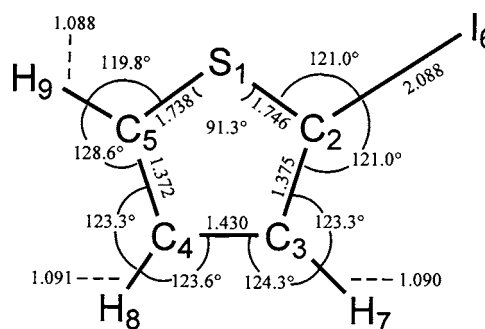

FIG. 1. B3LYP/Sadlej PVTZ computed geometry parameters of 2-iodothiophene (Cs symmetry) with bond lengths (in angstroms) and bond angles (in degrees) indicated.

electronic transition energies were calculated using B3LYP-TD/Sadlej cc-PVTZ. All of the density functional theory calculations made use of the GAUSSIAN program suite[90] The calculated normal modes and molecular orbitals were viewed with Molden and Gaussview software.

III. RESULTS AND DISCUSSION

A. Ground state geometry and vibrational spectra

Figure 1 shows a schematic diagram of the geometry of 2-iodothiophene with the atoms numbered and selected bond lengths and bond angles indicated. There appears to be no previous literature vibrational assignments made for the ground state of 2-iodothiophene. FT-Raman and FTIR measurements and B3LYP/Sadlej PVTZ computations were done to help determine the vibrational assignments for the ground state of 2-iodothiophene. Figure 2 displays the FT-Raman
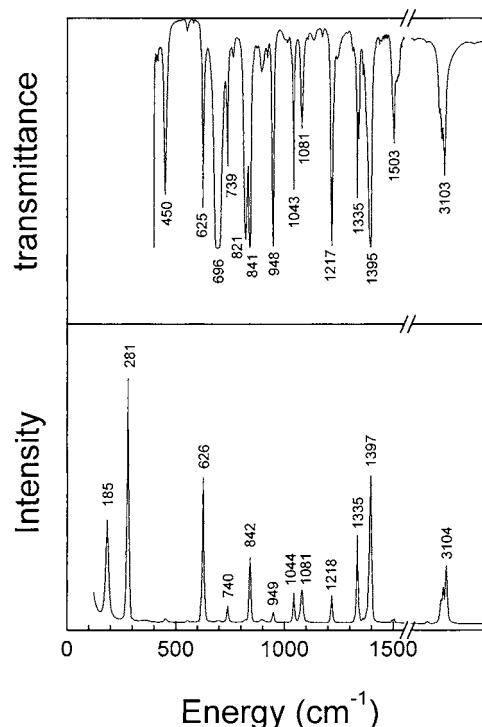

FIG. 2. FT-IR (top) and FT-Raman (bottom) spectra of neat 2-iodothiophene. The wave numbers (cm^{-1}) of the infrared bands and Raman shifts for the fundamental bands of interest are indicated above the vibrational bands (also see Table II for tentative vibrational assignments).

TABLE I. Experimental FTIR and FT-Raman vibrational bands and calculated vibrational frequencies for the ground state of 2-iodothiophene from B3LYP/Sadlej PVTZ calculations (vs, very strong; s, strong; m, medium; w, weak; vw, very weak).

Symmetry	No.	Calc.	b^a	Expt. FT-R	Expt. FT-IR	Assignments
A'	ν_1	3232	3112	3104 m	3103 m	C_5H stretch
	ν_2	3211	3092	3086 m	3086 m	C_3H stretch
	ν_3	3194	3076	3074 w	3072 m	C_4H stretch
	ν_4	1547	1504	1504 vw	1503 m	Antisymmetric C_2C_3/C_4C_5 stretch
	ν_5	1448	1410	1397 s	1395 vs	Symmetric C_2C_3/C_4C_5 stretch
	ν_6	1355	1321	1335 m	1335 m	HC_4/C_5H wag
	ν_7	1231	1202	1218 w	1217 vs	HC_3/C_4H wag
	ν_8	1088	1066	1081 w	1081 m	HC_4/C_5H scissor
	ν_9	1062	1041	1044 w	1043 s	HC_3/C_4H scissor
	ν_{10}	939	924	949 vw	948 vs	SC_2/C_2I stretch $+ SC_2C_3$ band
	ν_{11}	839	828	842 m	841 vs	SC_5 stretch $+ SC_5C_4$ bend
	ν_{12}	734	728	740 w	738 m	Antisymmetric CSC stretch
	ν_{13}	627	626	626 s	625 s	Symmetric CSC stretch
	ν_{14}	279	294	280 vs		CI stretch
	ν_{15}	186	205	185 m		ICS/ICC bend
A''	ν_{16}	926	911	896 vw	895 w	$HC_3/C_4H/C_5H$ twist
	ν_{17}	838	827	842 m	841 vs	$HC_3/C_4H/C_5H$ twist
	ν_{18}	701	697		694 vs	$HC_3/C_4H/C_5H$ rock
	ν_{19}	560	562	554 vw	552 vw	HC_3/C_4H twist
	ν_{20}	457	464	452 vw	450 s	Out-of-plane ring deformation
	ν_{21}	174	194			Out-of-plane I-ring bend

[a]Using the scaling equation scaled$=27.67+0.954\times$calculated.

(bottom) and the FTIR (top) spectra of 2-iodothiophene in the solid state. All 21 vibrational modes are both Raman and IR active. We have observed 20 vibrational modes from the FT-Raman and the FTIR spectra. Figure 2 shows that the FT-Raman and the FTIR spectra are complementary. Several Raman bands that are very weak at 450, 696, 821, 949, and 1503 cm^{-1} become strong or have moderate intensity in the FTIR spectrum. Table I lists the experimental and B3LYP/Sadlej PVTZ computed vibrational frequencies and lists their tentative assignments. There is generally good agreement between the calculated and experimental vibrational frequencies. We did not observe the calculated 179 cm^{-1} nominal out-of-plane I-ring bending mode (A'' representation) in the FT-Raman spectrum, probably because the actual Raman band is too weak or is too close to the 185 cm^{-1} band (A' representation) to be clearly seen.

B. Absorption spectrum

Figure 3 shows the absorption spectrum of 2-iodothiophene in cyclohexane solution with the excitation wavelengths for the resonance Raman experiments indicated above the spectrum. The B3LYP-TD/Sadlej PVTZ computed electronic transition energies and their oscillator strengths for 2-iodothiophene show that 2-iodothiophene has an electronic transition allowed band at about 255 nm with an oscillator strength $f=0.1635$ (for details see Table I in web-based materials). This is in good agreement with the experimentally measured oscillator strength of $f=0.175$ for the experimental 243 nm absorption band of the 2-iodothiophene molecule. The two orbitals that are involved in the electronic transition

associated with the calculated 255 nm absorption band of the 2-iodothiophene molecule are the highest occupied molecular orbital (HOMO) orbital that is mainly composed of the $p\pi$ orbital of iodine atom and the π orbital of the thiophene ring, and the lowest unoccupied molecular orbital (LUMO) +1 orbital that is characteristically the π^* orbital of the thiophene ring based on a semiempirical viewpoint (see Fig. 1 in web-based materials). Further natural-orbital analysis (using MOLDEN/MIX software) shows that HOMO orbital (using a contour value of 0.03) is more likely a nonbonding $p\pi$ orbital, whereas LUMO+1 orbital is the π^* orbital of the thiophene ring. We thus assign the strong experimental 243 nm absorption band to the $p\pi$ (I atom) $\rightarrow \pi^*$ (thiophene ring) electronic transition of 2-iodothiophene based on our present time-dependent density functional theory computa-
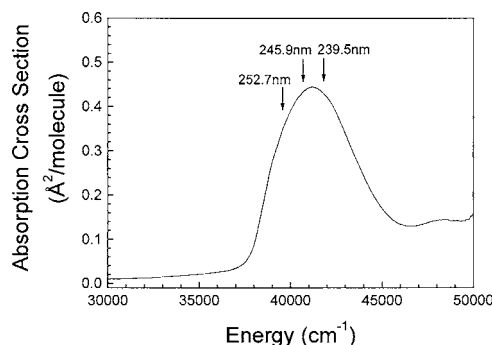
FIG. 3. Ultraviolet absorption spectrum of 2-iodothiophene in cyclohexane solution. The excitation wavelengths used for the resonance Raman experiments are indicated above the absorption spectrum.
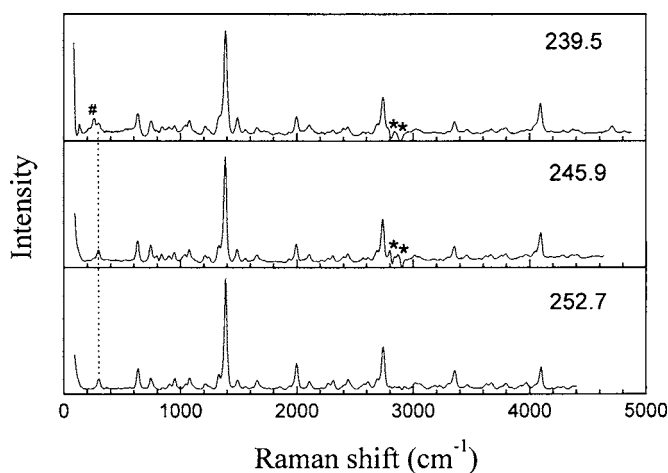
FIG. 4. Overview of the *A*-band resonance Raman spectra of 2-iodo-thiophene in cyclohexane solvent obtained with the excitation wavelengths (in nanometers) indicated next to each spectrum. The spectra have been intensity corrected and solvent subtracted (asterisks mark regions where solvent subtraction artifacts are present).

tions. The 245.9, 239.5, and 252.7 nm excitation wavelengths used in the resonance Raman experiments are in resonance with this 243 nm CT-band absorption of the 2-iodothiophene molecule.

C. Resonance Raman spectra

Figure 4 shows an overall view of the *A*-band resonance Raman spectra of 2-iodothiophene in cyclohexane solvent obtained with 239.5, 245.9, and 252.7 nm excitation wavelengths. Figure 5 presents an expanded view of the resonance Raman spectrum obtained with 245.9 nm excitation with tentative vibrational assignments indicated above the spectrum. The spectra shown in Figs. 4 and 5 have been corrected for sample reabsorption as well as the wavelength dependent response of the detection system. Solvent Raman bands were
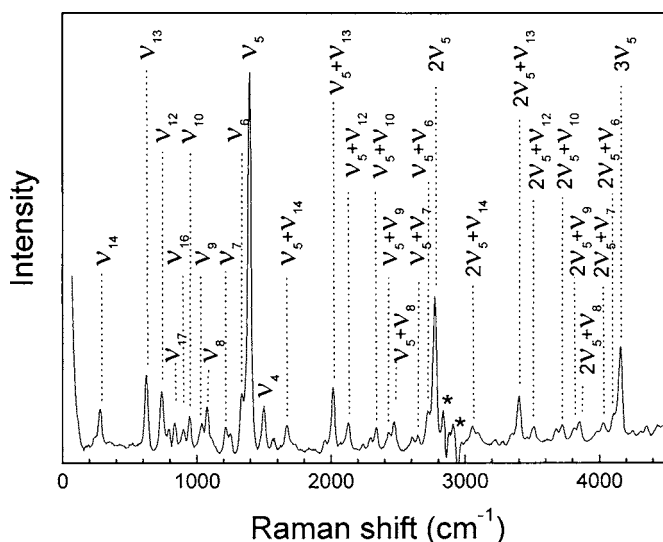

FIG. 5. Expanded view of the 245.9 nm resonance Raman spectrum of 2-iodothiophene in cyclohexane solvent. The spectrum has been intensity corrected and solvent subtracted. Asterisks label parts of the spectrum where solvent subtraction artifacts are present. The tentative assignments to the larger Raman band features are also shown.

removed from the spectra by subtracting an appropriately scaled solvent spectrum and regions and the solvent subtraction artifacts are indicated by asterisks. We note that the intensity of some Raman bands in the spectrum may have contributions from several Raman bands that have very close Raman shifts due to the limited resolution of the solution phase spectra. Thus, the Raman band labels in Fig. 5 only give the largest Raman band contributions to each Raman feature. Most of the resonance Raman features can be assigned to the fundamentals, overtones, and combination bands of about 11 vibrational modes based on the information in Table I: the nominal asymmetric C==C stretch ν_4 (1499 cm^{-1}), the nominal symmetric C==C stretch ν_5 (1397 cm^{-1}), the nominal HC$_4$C$_5$H rock ν_6 (1335 cm^{-1}), the nominal HC$_3$C$_4$H rock ν_7 (1217 cm^{-1}), the nominal HC$_4$C$_5$H scissor ν_8 (1081 cm^{-1}), the nominal HC$_3$C$_4$H scissor ν_9 (1043 cm^{-1}), the nominal SC$_2$/C$_2$I stretch+SC$_2$C$_3$ bend ν_{10} (948 cm^{-1}), the nominal SC$_5$ stretch+SC$_5$C$_4$ bend ν_{11} (841 cm^{-1}), the nominal antisymmetric CSC stretch ν_{12} (738 cm^{-1}), the nominal symmetric CSC stretch ν_{13} (626 cm^{-1}), and the nominal CI stretch ν_{14} (280 cm^{-1}).

D. Time-dependent wave packet calculations to model the *A*-band 245.9 and 252.7 nm resonance Raman intensities and absorption spectrum

We have chosen to model the relative intensities of the 245.9 and 252.7 nm resonance Raman spectra since they are clearly mostly on resonance with the *A*-band absorption. The 245.9 and 252.7 nm resonance Raman spectra have progressions of the nominal C$_2$C$_3$/C$_4$C$_5$ symmetric stretch ν_5 (1397 cm^{-1}) and its overtones as well as its combination bands with the nominal antisymmetric CSC stretch ν_{12} (738 cm^{-1}), the nominal symmetric CSC stretch ν_{13} (626 cm^{-1}), the nominal CI stretch ν_{14} (280 cm^{-1}), and seven other vibrational modes ν_{11}, ν_{10}, ν_9, ν_8, ν_7, ν_6, and ν_4. The absorption spectra and absolute resonance Raman cross sections were simulated using the time-dependent wave packet calculations and the simple model described in the Experimental and Computational Methods section. Table II presents the calculated parameters that best fit the data for 2-iodothiophene in the liquid absorption spectra and the intensities of the resonance Raman spectra. In order to simultaneously fit the absorption bandwidth and the pattern of the resonance Raman intensities, we needed to include a moderate amount of electronic dephasing (the Γ parameter) in the calculations that is similar to our previous work on gas and solution phase *A*-band iodoalkanes.[54–65] This indicates that the population decay/electronic dephasing occurs substantially faster than just wave packet motion away from the Franck-Condon region.

Since the *A*-band resonance Raman spectra of 2-iodothiophene could possibly be susceptible to interference from preresonance-resonance effects[52,57,86] from higher energy states, we have given greater weight to fitting the larger overtones and combination band features. The top part of Fig. 6 shows a comparison of the calculated absorption spectrum (dotted line) with the experimental (solid line) absorption spectrum. Figure 6 (and Table II in web-based materials)

TABLE II. Parameters for the time-dependent wave packet calculations for 2-iodothiophene.

Vibrational Mode		Ground state vibrationa frequency (cm^{-1})	$|\Delta|$	Vibrational reorganization energy (cm^{-1})
ν_{14}	ν_{C-I} stretch	296	1.47	320
ν_{13}	Symmetric CSC stretch	635	1.25	496
ν_{12}	Antisymmetric CSC stretch	746	0.92	316
ν_{11}	SC_5 stretch+SC_5C_4 bend	846	0.48	97
ν_{10}	SC_2/C_2I stretch+SC_2C_3	950	0.52	128
ν_9	HC_3/C_4H scissor	1037	0.55	157
ν_8	HC_4/C_5H scissor	1078	0.59	188
ν_7	HC_3/C_4H wag	1213	0.37	83
ν_6	HC_4/C_5H wag	1327	0.50	166
ν_5	Symmetric C_2C_3/C_4C_5 stretch	1388	1.48	1520
ν_4	Antisymmetric C_2C_3/C_4C_5 stretch	1488	0.30	67

Transition length $M=0.94$ å, $E_0=38\ 100\ cm^{-1}$, $\Gamma=270\ cm^{-1}$, Total$=3538\ cm^{-1}$

also shows a comparison of the calculated resonance Raman cross sections (open bars) with the experimental Raman cross sections (solid bars) for the 20 main Raman features of the 245.9 and 252.7 nm resonance Raman spectra.

Inspection of Fig. 6 shows that there is reasonable agreement between the calculated and experimental absorption spectra and that the calculated spectrum is consistent with the oscillator strength of the *A*-band transition. There is also a good fit to the absolute Raman intensities of the 245.9 and 252.7 nm spectra as shown in lower part of Fig. 6. If any of the parameters in Table II are changed beyond their estimated uncertainties (about $\pm 5\% - 10\%$) the calculated fit to the absorption spectrum and/or resonance Raman cross section becomes noticeably poorer. The overall best fit to both the absorption spectrum and the absolute resonance Raman intensities appears to be reasonable enough to help determine the major features of the transition and its associated short-time dynamics on the excited state potential energy surface.

Examination of the $|\Delta|$ dimensionless parameters (or vibrational reorganizational energies λ_v) determined by fitting the absorption spectrum and the resonance Raman cross sections shows that the largest changes in the displacements occur with the nominal C_2C_3/C_4C_5 symmetric stretch mode ν_5 ($|\Delta|=1.48$, $\lambda=1520\ cm^{-1}$). There are also modes contributions from the nominal symmetric CSC stretch mode ν_{13} ($|\Delta|=1.25$, $\lambda=496\ cm^{-1}$), the nominal C–I stretch mode ν_{14} ($|\Delta|=1.47$, $\lambda=320\ cm^{-1}$), the nominal asymmetric CSC stretch ν_{12} ($|\Delta|=0.92$, $\lambda=316\ cm^{-1}$), and other seven mode ν_{11}, ν_{10}, ν_9, ν_8, ν_7, ν_6, and ν_4 ($|\Delta|=0.3-0.6$, $\lambda=190-60\ cm^{-1}$). Our results indicate that the short-time photodissociation dynamics of 2-iodothiophene have significant multidimensional character predominantly in the nominal C_2C_3/C_4C_5 symmetry stretch mode ν_5. This large overtone progression ($n\nu_5$) is accompanied by moderate contributions from the fundamentals and combination bands of the nominal CSC symmetric/antisymmetric mode ν_{13}/ν_{12} and the nominal C–I stretch mode ν_{14}, as well as by smaller contributions from the ν_{11}, ν_{10}, ν_9, ν_8, ν_7, ν_6, and ν_4 vibrational modes.

E. The *A*-band 2-iodothiophene photodissociation dynamics and comparison to previous work on iodobenzene

The *A*-band absorption and resonance Raman spectra of 2-iodothiophene are similar to those of iodobenzene. The absorption spectrum of iodobenzene in the 200–350 nm region has been well characterized.[68,69,91,92] The absorption band of iodobenzene at ~260 nm was attributed to the $n \rightarrow \sigma^*$ transition of the C–I bond (this is also known as the *A*-band absorption), whereas the band in the 220–230 nm region was assigned to the $\pi \rightarrow \pi^*$ transition of the benzene ring (this is also known as the *B*-band absorption). The *B*-band absorption of iodobenzene (oscillator strength of $f=0.211$) is assigned to an electron transfer from the nonbonding iodine orbital ($5p\pi$) to the lowest unoccupied benzene orbital.[91] Similarly the *A*-band absorption of 2-iodothiophene (maximum at about 243 nm with an oscillator strength of $f=0.175$) is also characteristically assigned to the $p\pi$ (I atom)$\rightarrow \pi^*$ (thiophene ring) electron transition based on our present time-dependent density functional theory calculations. The similar $p\pi$ (I atom)$\rightarrow \pi^*$ (thiophene or benzene ring) electron transition for the two absorption bands of 2-iodothiophene and iodobenzene leads to a similar resonance Raman intensity pattern for both molecules. Bonang and Cameron[79] and Kung *et al.*[78(a)] reported that the *B*-band resonance Raman spectrum of iodobenzene had most of the Raman band intensity in Raman bands associated with the nominal C=C ring stretch ν_{8a} mode (1583 cm^{-1}), the nominal total symmetric ring breathing mode ν_1 (1002 cm^{-1}), the β_{C-H} mode ν_{7a} (1057 cm^{-1}), the ν_{9a} (1176 cm^{-1}), the $\nu_{C=C}$ mode ν_{19a} (1464 cm^{-1}), and their binary overtones and combination bands. The C=C ring stretch ν_{8a} mode makes the predominant contribution to the resonance Raman spectrum of iodobenzene, with noticeable Raman bands associated with the ν_1, ν_{7a}, ν_{8a}, and ν_{9a} vibrational modes. This is similar to the resonance Raman intensity pattern observed for 2-iodothiophene where most of the Raman intensity is along the skeletal modes of the thienyl ring in this work.
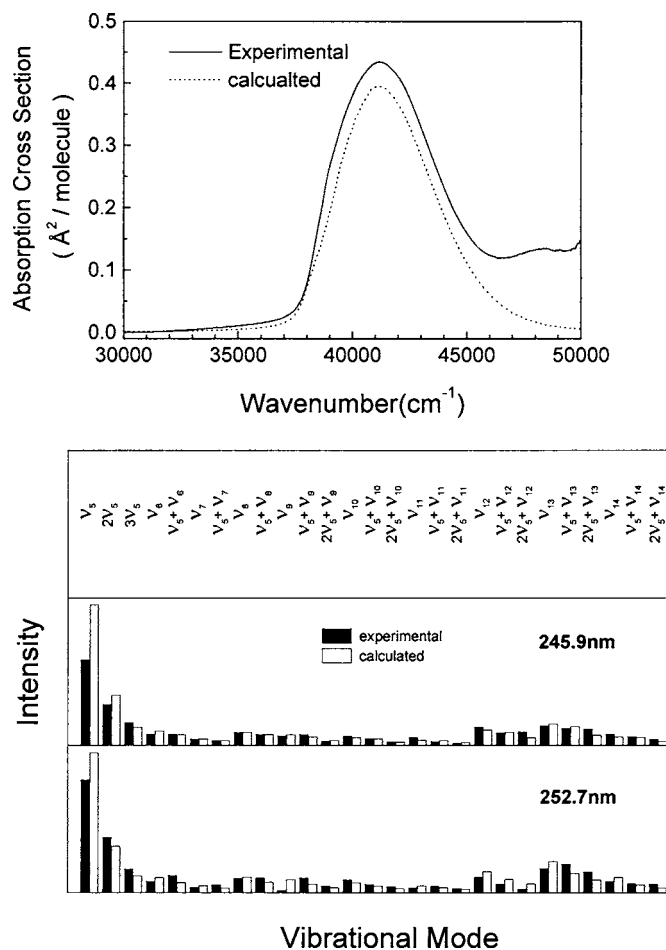
Further examination of the 229 nm resonance Raman

FIG. 6. (Top) Comparison of the computed absorption spectrum (dotted line) with the experimental (solid line) absorption spectrum. (Bottom) Comparison of the computed resonance Raman cross sections (open bars) with the experimental Raman cross sections (solid bars) for the main Raman features of the 245.9 and 252.7 nm resonance Raman spectra. The computations made use of the model described in Refs. 18, 19, and 46 with a simple exponential decay dephasing treatment for the solvent (see text for details).

spectrum of iodobenzene[78(b)] and the A-band resonance Raman spectra of 2-iodothiophene shows some interesting differences. Firstly the intensity of the nominal C–I stretch mode at 265 cm^{-1} is as strong as the nominal C=C ring stretch ν_{8a} mode (1583 cm^{-1}) for iodobenzene.[78(b)] This indicates that the excited state geometry undergoes substantial change along the C–I coordinate besides the major changes that occur along the benzene ring skeletal motions. In contrast, the intensity of the nominal C–I stretch mode ν_{14} (296 cm^{-1}) is much weaker than the C=C stretch mode for 2-iodothiophene. The vibrational reorganizational energies for the C=C symmetric stretch mode and the C–I stretch mode are 1520 and 320 cm^{-1}, respectively. The significant difference between the vibrational reorganizational energies distributed to the C–I stretch mode relative to the symmetric C=C stretch mode for the 2-iodothiophene and iodobenzene molecules may be due to differences induced by the structural and electronic differences in the thienyl ring and benzene rings. A curve crossing mechanism was proposed for the photodissociation dynamics of iodobenzene.[72–74,77] Using a 278 nm pump wavelength, excitation of iodoben-

zene takes it to the $^3(\pi,\pi^*)$ state and this makes the phenyl ring become vibrationally excited. With this high total vibrational energy taking place in the $^3(\pi,\pi^*)$ phenyl ring modes, the C–I mode can quickly become excited through intramolecular vibrational redistribution. This is then followed by a strong coupling to the repulsive $^3(n,\sigma^*)$ surfaces, leading to the cleavage of the C–I bond. We note from recent papers that similar curve crossings exist in the chlorobenzene and bromobenzene molecular systems. Sobolewski and Domcke proposed a $^1(\pi,\pi^*)$–$^1(\pi,\sigma^*)$ conical intersection along C–Cl bond length for chlorobenzene, where the $^1(\pi,\sigma^*)$ surface is repulsive and causes the C–Cl bond to dissociate.[70] Rasmusson $et\ al.$ predicted a possible $^1(\pi,\pi^*)$–$^3(\pi,\pi^*)$ curve crossing channel for the C–Br bond breaking mechanism of bromobenzene, where $^3(\pi,\pi^*)$ state is repulsive along the C–Br bond length.[71] Due to the spin-orbital coupling, we think that both the $^1(\pi,\pi^*)$–$^1(\pi,\sigma^*)$ curve crossing and the $^1(\pi,\pi^*)$–$^3(\pi,\pi^*)$ curve crossings are possible for iodobenzene. The enhancement in the C=C stretch and other ring skeletal vibrational mode as well as the considerable intensity in the C–I stretch mode for the 229 nm resonance Raman spectrum of iodobenzene suggest that before a possible curve crossing takes place, both the benzene ring and the C–I bond undergo noticeable change along these coordinates. The noticeable geometry change in the C–I bond for iodobenzene is consistent with a dissociating triplet state along a $C–X$ coordinate. In contrast, our resonance Raman intensity analysis results indicate that the C–I bond length change for 2-iodothiophene is much less than that for iodobenzene. This suggests that before a similar curve crossing can take place much of the vibrational energy is partitioned to the skeletal vibrations rather than to the C–I motion. This would suggest that the potential energy surface that intersects with the initial $^1(\pi,\pi^*)$ potential of 2-iodothiophene would not be very repulsive along the C–I coordinate. Recently we have carried out an UV-photolysis study of 2-iodothiophene by using the matrix isolation infrared (IR) method. The thienyl radical was not detected. Instead another transient species was found that did not appear to be produced from the thienyl radical reaction channel. This suggests that the C–I bond photodissociation may not occur for 2-iodothiophene via a pathway similar to that of iodobenzene. The smaller normal mode displacement of the C–I stretch mode in the A-band Franck-Condon region of 2-iodothiophene may indicate that the excited state that possibly intersects with the $^1(\pi,\pi^*)$ state would not necessarily be dissociative nor be the major dissociative channel along the C–I coordinate for 2-iodothiophene.

It is very interesting to note from Table II that there are two coupled symmetric and antisymmetric normal modes: the symmetric and antisymmetric C=C stretches (ν_5 and ν_4) and the symmetric and antisymmetric CSC stretches (ν_{13} and ν_{12}). Due to the combination of normal mode displacements for each pair of modes (ν_5 and ν_4 or ν_{13} and ν_{12}), the Franck-Condon region geometry change along the two C=C or C–S bonds will be different. Since the normal mode displacement for the antisymmetric C=C stretch ν_4 is very small, the two C=C bond length changes would be expected to become larger or shorter simultaneously. However,

the normal mode displacement for the antisymmetric C–S stretch ν_{12} is considerably larger ($|\Delta|=0.92$, $\lambda=316$ cm^{-1}) and is comparable to that ($|\Delta|=1.25$, $\lambda=496$ cm^{-1}) for the symmetric C–S stretch mode. This indicates that the bond length changes along the two C–S coordinates are significantly different in the Franck-Condon region, with one C–S bond length becoming longer while the other C–S bond length becoming shorter. The subtotal vibrational reorganizational energy for these two modes is 812 cm^{-1} (about 23% of the total vibrational reorganizational energy) and this is larger than vibrational reorganizational energy for the C–I stretch mode (320 cm^{-1}, 9% of the total vibrational reorganizational energy). This suggests that a possible curve crossing between the $^1(\pi,\pi^*)$ state and some other excited state that is dissociative along the C–S coordinate may be more likely. D'Auria proposed a photoisomerization and singlet-triplet intersystem crossing mechanism for the photochemical reaction of thiophene derivatives.[83] If the first excited singlet state of a thiophene derivative molecule is populated, the molecule can be converted into the corresponding triplet state that undergoes further $X-C_\alpha$ bond cleavage to produce ring opening products or change into the corresponding Dewar isomer depending on the energetic factors of the reaction pathways. The curve crossing of the singlet excited state to the triplet excited state of thiophene is not likely to occur. However, the intersystem crossing from the initially populated singlet excited state to the triplet excited state can probably occur for thiophene-2-carbonitrile. Our Franck-Condon photochemical reaction dynamics indicate that the two C–S bonds undergo significantly different bond length changes for 2-iodothiophene in its initially excited state. This suggests that this excited state may have a character more consistent with one that could undergo a singlet-triplet intersystem crossing mechanism that is thiophene-2-carbonitrile in nature.

Further investigations are needed to better clarify the possible curve crossing between the $^1(\pi,\pi^*)$ state and the $^3(\pi,\pi^*)$ state that is dissociative along the C–S coordinate. Advanced quantum mechanical computations, such as complete active space self-consistent field (CASSCF) and CASPT2, could be helpful to locate important intersystem crossing points between the initial $^1(\pi,\pi^*)$ state and various other excited states (singlets or triplets, dissociative, or bound) along the major Franck-Condon active modes. The short-time dynamics in terms of the internal coordinate changes would also be useful to quantitatively examine how the Franck-Condon region geometry changes correlate with the possible curve crossing between the initial $^1(\pi,\pi^*)$ state and other excited states. Other experimental investigations such as femtosecond time-resolved electron diffraction spectroscopy, femtosecond time-resolved absorption spectra, femtosecond time-resolved pump-probe experiments, time-of-flight molecular beam experiments, and other experiments would also be very useful to better understand the *A*-band photodissociation dynamics and photochemistry of 2-iodothiophene. Such experiments would help elucidate how different substituents influence the photodissociation dynamics and photochemistry of aromatic halides.

IV. CONCLUSION

A-band resonance Raman spectra were acquired for 2-iodothiophene in cyclohexane solution and a preliminary resonance Raman intensity analysis was done. The resonance Raman spectra and an intensity analysis of these spectra indicate that most of the short-time photodissociation dynamics in the Franck-Condon region occur along the nominal C_2C_3/C_4C_5 symmetric stretch the nomicalmode ν_5 ($|\Delta|=1.48$, $\lambda=1520$ cm^{-1}), the nominal symmetric CSC stretch mode ν_{13} ($|\Delta|=1.25$, $\lambda=496$ cm^{-1}), the nominal C–I stretch mode ν_{14} ($|\Delta|=1.47$, $\lambda=320$ cm^{-1}), and the nominal asymmetric CSC stretch ν_{12} ($|\Delta|=0.92$, $\lambda=316$ cm^{-1}). These are also smaller components along other seven modes ν_{11}, ν_{10}, ν_9, ν_8, ν_7, ν_6, and ν_4 (with $|\Delta|=0.3-0.6$, $\lambda=190-60$ cm^{-1}). These results for 2-iodothiophene were compared to those previously reported for iodobenzene and iodoalkanes. The resonance Raman intensity pattern for 2-iodothiophene is similar to that for iodobenzene and indicates that most of the available vibrational energy is partitioned to the skeletal vibrational motions for 2-iodothiophene. This energy partitioning is very different than those previously determined for iodoalkanes where most of the available vibrational energy takes place in the C–I stretch. The Franck-Condon region geometry changes along the two C–S bonds in 2-iodothiophene are found to be very different, with one C–S bond length becoming longer while the other C–S bond length becoming shorter. The Franck-Condon region geometry change along the C–I bond for 2-iodothiophene is also found to be not only much smaller than that for iodobenzene but also considerably smaller than that of the two C–S bonds. These differences combined with our recent matrix-isolation IR experiment as well as the comparison to CASPT2 computations on the curve crossing of iodobenzene suggest that a possible curve crossing between the $^1(\pi,\pi^*)$ state and some excited state that is dissociative along the C–S coordinate may be more likely for 2-iodothiophene.

[1] A. Gedanken and M. D. Rowe, Chem. Phys. Lett. **34**, 39 (1975).
[2] J. L. Knee, L. R. Khundar, and A. H. Zewail, J. Chem. Phys. **83**, 1996 (1985).
[3] L. R. Khundar and A. H. Zewail, Chem. Phys. Lett. **142**, 426 (1987).
[4] R. K. Sparks, K. Shobatake, L. R. Carlson, and Y. T. Lee, J. Chem. Phys. **75**, 3838 (1981).
[5] G. N. A. Van Veen, T. Baller, A. E. Devries, and N. J. A. Van Veen, Chem. Phys. **87**, 405 (1984).
[6] I. Powis and J. F. Black, J. Phys. Chem. **93**, 2461 (1989).
[7] R. Ogorzalek-Loo, H.-P. Haerri, G. E. Hall, and P. L. Houston, J. Chem. Phys. **90**, 4222 (1989).
[8] D. W. Chandler, M. H. M. Janssen, S. Stolte, R. N. Strickland, J. W. Thoman, Jr., and D. H. Parker, J. Phys. Chem. **94**, 4839 (1990).
[9] G. E. Hall, T. J. Sears, and J. M. Frye, J. Chem. Phys. **89**, 580 (1988).
[10] N. E. Triggs, M. Zahedi, J. W. Nibler, P. A. Debarber, and J. J. Valentini, J. Chem. Phys. **96**, 2756 (1992).

[11] S. J. Riley and K. R. Wilson, Faraday Discuss. Chem. Soc. **53**, 132 (1972).

[12] M. K. Dzvonik, S. Yang, and R. Bersohn, J. Chem. Phys. **61**, 4408 (1974).

[13] M. Kawasaki, S. J. Lee, and R. Bersohn, J. Chem. Phys. **63**, 809 (1975).

[14] P. M. Kroger, P. C. Demou, and S. J. Riley, J. Chem. Phys. **65**, 1823 (1976).

[15] T. K. Minton, P. Felder, R. J. Brudzynski, and Y. T. Lee, J. Chem. Phys. **81**, 1759 (1984).

[16] D. Krajnovitch, L. J. Butler, and Y. T. Lee, J. Chem. Phys. **81**, 3031 (1984).

[17] G. N. A. Van Veen, T. Baller, A. E. DeVries, and M. Shapiro, Chem. Phys. **93**, 277 (1985).

[18] Q.-X. Xu, K.-H. Jung, and R. B. Bernstein, J. Chem. Phys. **89**, 2099 (1988).

[19] W. K. Kang, K. W. Jung, D. C. Kim, K.-H. Jung, and H. S. Im, Chem. Phys. **196**, 363 (1995).

[20] W. K. Kang, K. W. Jung, D.-C. Kim, and K.-H. Jung, J. Chem. Phys. **104**, 5815 (1995).

[21] R. J. Donovan, F. G. M. Hathorn, and D. Husain, Trans. Faraday Soc. **64**, 3192 (1968).

[22] T. F. Hunter, S. Lunt, and K. S. Kristjansson, J. Chem. Soc., Faraday Trans. 2 **79**, 303 (1983).

[23] E. Gerck, J. Chem. Phys. **79**, 311 (1983).

[24] S. Uma and P. K. Das, Can. J. Chem. **72**, 865 (1994).

[25] D. H. Fairbrother, K. A. Briggman, E. Wietz, and P. C. Stair, J. Chem. Phys. **101**, 3787 (1994).

[26] P. L. Ross and M. V. Johnston, J. Phys. Chem. **99**, 4078 (1995).

[27] S. Uma and P. K. Das, Chem. Phys. Lett. **241**, 335 (1995).

[28] S. Uma and P. K. Das, J. Chem. Phys. **104**, 4470 (1996).

[29] M. Shapiro and R. Bersohn, J. Chem. Phys. **72**, 3810 (1980).

[30] S. K. Gray and M. S. Child, Mol. Phys. **51**, 189 (1984).

[31] M. Shapiro, J. Phys. Chem. **90**, 3644 (1986).

[32] M. Tadjeddine, J. P. Flament, and C. Teichteil, Chem. Phys. **118**, 45 (1987).

[33] H. Guo and G. C. Schatz, J. Chem. Phys. **93**, 393 (1990).

[34] Y. Amatatsu, K. Morokuma, and S. Yabushita, J. Chem. Phys. **94**, 4858 (1991).

[35] H. Guo and G. C. Schatz, J. Chem. Phys. **95**, 3091 (1991).

[36] H. Guo, J. Chem. Phys. **96**, 2731 (1992).

[37] A. D. Hammerich, U. Manthe, R. Kosloff, H.-D. Meyer, and L. S. Cederbaum, J. Chem. Phys. **101**, 5623 (1994).

[38] Y. Amatatsu, S. Yabushita, and K. Morokuma, J. Chem. Phys. **104**, 9783 (1996).

[39] D. G. Imre, J. L. Kinsey, A. Sinha, and J. Krenos, J. Phys. Chem. **88**, 3956 (1984).

[40] M. O. Hale, G. E. Galica, S. G. Glogover, and J. L. Kinsey, J. Phys. Chem. **90**, 4997 (1986).

[41] G. E. Galica, B. R. Johnson, J. L. Kinsey, and M. O. Hale, J. Phys. Chem. **95**, 7994 (1991).

[42] K. Q. Lao, M. D. Person, P. Xayaroboun, and L. J. Butler, J. Chem. Phys. **92**, 823 (1990).

[43] F. Markel and A. B. Myers, Chem. Phys. Lett. **167**, 175 (1990).

[44] A. B. Myers and F. Markel, Chem. Phys. **149**, 21 (1990).

[45] F. Markel and A. B. Myers, J. Chem. Phys. **98**, 21 (1993).

[46] P. G. Wang and L. D. Zeigler, J. Phys. Chem. **97**, 3139 (1993).

[47] B. R. Johnson and J. L. Kinsey, J. Phys. Chem. **100**, 18937 (1996).

[48] F. Duschek, M. Schmitt, P. Vogt, A. Materny, and W. Kiefer, J. Raman Spectrosc. **28**, 445 (1997).

[49] J. Zhang and D. G. Imre, J. Chem. Phys. **89**, 309 (1988).

[50] D. L. Phillips, B. A. Lawrence, and J. J. Valentini, J. Phys. Chem. **95**, 7570 (1991).

[51] D. L. Phillips, B. A. Lawrence, and J. J. Valentini, J. Phys. Chem. **95**, 9085 (1991).

[52] D. L. Phillips and A. B. Myers, J. Chem. Phys. **95**, 7164 (1991).

[53] D. L. Phillips, J. J. Valentini, and A. B. Myers, J. Phys. Chem. **96**, 2039 (1992).

[54] W. M. Kwok and D. L. Phillips, Chem. Phys. Lett. **235**, 260 (1995).

[55] D. L. Phillips and W. M. Kwok, Chem. Phys. Lett. **241**, 267 (1995).

[56] S. Q. Man, W. M. Kwok, and D. L. Phillips, J. Phys. Chem. **99**, 15705 (1995).

[57] W. M. Kwok and D. L. Phillips, J. Chem. Phys. **104**, 2529 (1996).

[58] W. M. Kwok and D. L. Phillips, J. Chem. Phys. **104**, 9816 (1996).

[59] S.-Q. Man, W. M. Kwok, A. E. Johnson, and D. L. Phillips, J. Chem. Phys. **105**, 5842 (1996).

[60] W. M. Kwok, P. K. Ng, G. Z. He, and D. L. Phillips, Mol. Phys. **90**, 127 (1997).

[61] D. L. Phillips and A. B. Myers, J. Raman Spectrosc. **28**, 839 (1997).

[62] X. Zheng and D. L. Phillips, Chem. Phys. Lett. **286**, 79 (1998).

[63] X. Zheng and D. L. Phillips, J. Chem. Phys. **108**, 5772 (1998).

[64] X. Zheng and D. L. Phillips, Chem. Phys. Lett. **292**, 295 (1998).

[65] D. L. Phillips, Prog. React. Kinet. **24**, 223 (1999) and references therein.

[66] M. Dzvonik, S. Yang, and R. Bersohn, J. Chem. Phys. **61**, 4408 (1974).

[67] A. Freedman, S. C. Yang, M. Kawasaki, and R. Bersohn, J. Chem. Phys. **72**, 1028 (1980).

[68] T. M. Dunn and T. Iredale, J. Chem. Soc. **1952**, 1592.

[69] R. A. Durie, T. Iredale, and J. M. S. Jarine, J. Chem. Soc. **1950**, 1181.

[70] A. L. Sobolewski and W. Domcke, Chem. Phys. **259**, 181 (2000).

[71] M. Rasmusson, R. Lindh, N. Lascoux, A. N. Tarnovsky, M. Kadi, O. Kühn, V. Sundström, and E. Åkesson, Chem. Phys. Lett. **367**, 759 (2003).

[72] H. J. Hwang and M. A. El-Sayed, J. Chem. Phys. **96**, 856 (1992).

[73] J. E. Freitas, H. J. Hwang, and M. A. El-Sayed, J. Phys. Chem. **97**, 12481 (1993).

[74] J. E. Freitas, H. J. Hwang, and M. A. El-Sayed, J. Phys. Chem. **98**, 3322 (1994).

[75] H. J. Hwang and M. A. El-Sayed, J. Photochem. Photobiol., A **102**, 13 (1996).

[76] J. A. Griffiths, K. W. Jung, and M. A. El-Sayed, J. Phys. Chem. **100**, 7989 (1996).

[77] P. Y. Cheng, D. Zhong, and A. H. Zewail, Chem. Phys. Lett. **237**, 399 (1995).

[78] (a) C.-Y. Kung, B.-Y. Chang, C. Kittrell, B. R. Johnson, and J. L. Kinsey, J. Phys. Chem. **97**, 2228 (1993); (b) S. C. O'Brien, C. Kittrell, J. L. Kinsey, and B. R. Johnson, J. Chem. Phys. **96**, 67 (1992); (c) R. Clark and A. J. McCaffery, J. Phys. Chem. **81**, 1918 (1977).

[79] C. C. Bonang and S. M. Cameron, Chem. Phys. Lett. **187**, 619 (1991).

[80] M. D'Auria, C. Distefano, F. D'Onofrio, G. Mauriello, and R. Racioppi, J. Chem. Soc., Perkin Trans. 1 **2000**, 3513.

[81] M. Novi, G. Garbarino, G. Petrillo, and C. Dell'Erba, J. Org. Chem. **52**, 5382 (1987).

[82] M. D'Auria, Gazz. Chim. Ital. **124**, 195 (1994).

[83] M. D'Auria, J. Photochem. Photobiol., A **149**, 31 (2002).

[84] S. A. Asher, Annu. Rev. Phys. Chem. **39**, 537 (1988).

[85] S. Y. Lee and E. J. Heller, J. Chem. Phys. **71**, 4777 (1979); E. J. Heller, R. L. Sundberg, and D. J. Tannor, J. Phys. Chem. **86**, 1822 (1982).

[86] A. B. Myers and R. A. Mathies, in *Biological Applications of Raman Spectroscopy*, edited by T. G. Spiro (Wiley, New York, 1987), Vol. 2, p. 1.

[87] A. B. Myers, in *Laser Techniques in Chemistry*, edited by A. B. Myers and T. R. Rizzo (Wiley, New York, 1995), p. 325.

[88] A. Becke, J. Chem. Phys. **84**, 4524 (1986).

[89] C. Lee, W. Yang, and R. G. Parr, Phys. Rev. B **37**, 785 (1988).

[90] M. J. Frisch, G. W. Trucks, H. B. Schlegel *et al.*, GAUSSIAN 98, Revision A.7, Gaussian, Inc., Pittsburgh, PA, 1998.

[91] K. Kimura and S. Nagakura, Mol. Phys. **9**, 117 (1965).

[92] J. P. Doering, J. Chem. Phys. **67**, 4065 (1977).